

Propagation Loss Measurements in Semiconductor Microcavity Ring and Disk Resonators

D. Rafizadeh, J. P. Zhang, R. C. Tiberio, and S. T. Ho

Abstract—We report the measurement of cavity propagation losses in nearly single-mode semiconductor waveguide-coupled ring and disk microcavity optical resonators. Using a novel 10.5- μm -diameter ring resonator, we measure transverse electric (TE) and transverse magnetic (TM) field intensity losses in 0.35- μm -wide ring waveguide cavities in the 1.55- μm -wavelength region. We present the experimental results for nanofabricated AlGaAs/GaAs 10.5- μm -diameter ring and disk resonators to quantify cavity losses and to show the feasibility of these promising and robust submicron-scale devices.

Index Terms—Integrated optics, loss measurement, microresonators, optical device fabrication, optical filters, optical waveguides.

I. INTRODUCTION

ADVANCES in fabrication technology have made it possible to create micrometer-size photonics devices based on reasonably low-loss semiconductor waveguides. Low-loss semiconductor waveguides are the building blocks of many integrated filters, switches, modulators, and multiplexers, and they can be combined with laser sources in the 1.3–1.6- μm wavelength range (such as lasers based on the InGaAsP/InP material system). In addition to device applications, strongly confined low-loss waveguides can also allow sharp S-turns which are necessary to form very compact, highly integrated circuitry.

Since the propagation loss is a critical factor in the performance of these devices, we examine propagation losses in nanofabricated, submicron-wide waveguide cavities and identify the sources and magnitudes of loss. Throughput is good general indicator of loss in waveguides, but coupling losses (e.g., from end-firing into the waveguides) are often difficult to separate from actual propagation losses. High- Q microcavity ring and disk resonators provide an accurate measure of waveguide loss and can be designed for nearly single-mode operation. The measured finesse and maximum transmission parameters directly determine the cavity losses and coupling.

Manuscript received November 13, 1997; revised April 6, 1998. This work was supported by AFOSR/ARPA under Contract F49620-96-1-0262 and by the NSF Faculty Early Career Development Award ECS-9502475.

D. Rafizadeh was with Northwestern University, Evanston, IL 60208 USA. She is now with The Aerospace Corporation, Photonics Technology Department, El Segundo, CA 90245 USA.

J. P. Zhang and S. T. Ho are with the Department of Electrical and Computer Engineering, McCormick School of Engineering, Northwestern University, Evanston, IL 60208 USA.

R. C. Tiberio is with Cornell Nanofabrication Facility, Cornell University, Ithaca, NY 14853 USA.

Publisher Item Identifier S 0733-8724(98)04834-8.

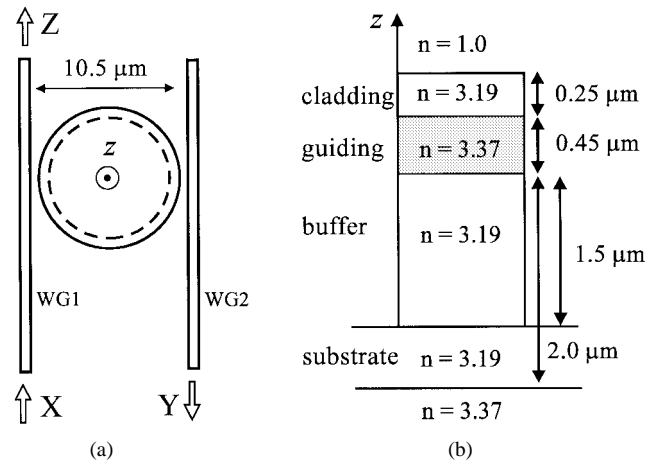


Fig. 1. (a) Illustration of the ring or disk resonator geometry and (b) schematic of the vertical waveguide structure and composition.

Previous integrated waveguide-type ring-geometry resonator devices are typically large cavity structures (>1 mm radius) based on weakly guiding waveguides [1]–[7]. Weakly guiding single-ring resonators have been used for propagation loss measurements in low-loss silica-based waveguides [1]–[6] and in polymer waveguides [7]. The weakly guiding ring resonators are created by a very small difference (e.g., $\Delta n = 0.02$) between the index of refraction of the core and cladding. Due to the low index contrast, there is high curvature-induced bending loss, and the rings are limited to large radii of curvature. As for device considerations, since the free spectral range $\Delta\lambda_{\text{fsr}}$ is inversely proportional to the cavity size, the $\Delta\lambda_{\text{fsr}}$ cannot be very wide due to the large cavity size of the rings.

Recently, the microcavity waveguide-coupled resonator has been experimentally realized by our group [8], [9] and two others [10], [11]. By etching through the guiding layer, it is possible to create very strong lateral waveguide confinement resulting from the high index contrast between the core (semiconductor) and cladding (air) layers. The resonator diameter can then be of the order of a few micrometers in diameter with negligible curvature-induced bending losses. The small cavity size results in a wide $\Delta\lambda_{\text{fsr}}$ and high cavity Q due to low cavity losses. We have measured 10.5- μm -diameter disk resonators with $\Delta\lambda_{\text{fsr}}$ of approximately 22 nm and Q of nearly 9000 [8], [9]. The geometry is illustrated in Fig. 1(a). Light entering port X is switched to port Y if it is on resonance with the resonator or exits from port Z if it is off resonance.

Transmission and reflection resonances, as well as the associated cavity losses, are presented here for nanofabri-

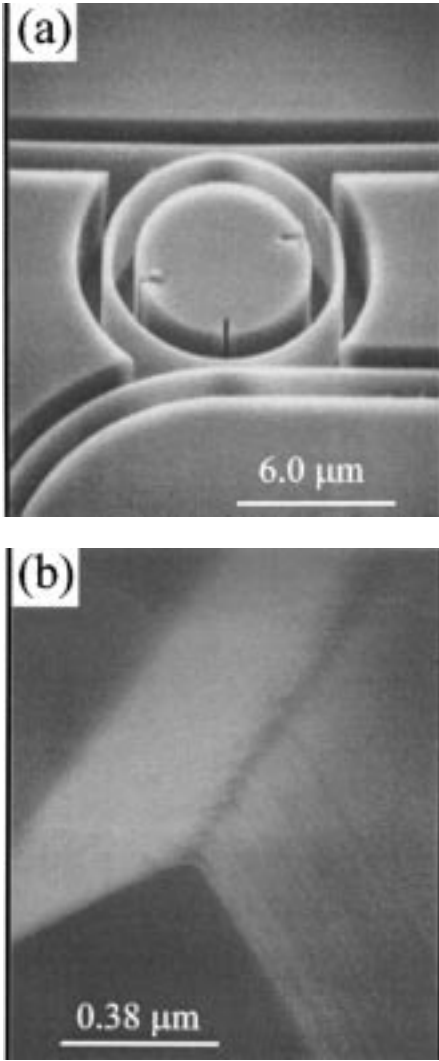


Fig. 2. SEM images of (a) the AlGaAs/GaAs 10.5- μm -diameter ring resonator composed of 0.35- μm -wide waveguides and gap separation of 0.12 μm and (b) a close-up of a cleaved waveguide end facet.

cated 10.5- μm -diameter ring resonators for both transverse electric (TE) and transverse magnetic (TM) polarizations. The resonator is composed of a ring waveguide and adjacent side-coupled waveguides which are 0.35 μm wide. The small resonator cavity maintains a reasonably high finesse even with high propagation losses, allowing the measurement of these losses with good accuracy. We have also experimentally realized the disk microcavity resonator in addition to the ring resonator. The disk resonator confines the light as well as the ring resonator but has lower cavity scattering loss since only the outer sidewall is etched, and there is no etched inner sidewall to contribute further to scattering losses.

II. RESONATOR PARAMETERS AND LOSS MECHANISMS

With each round-trip in the cavity, overlapping waves in the resonator cavity must be in phase, meaning that the phase difference of each round-trip must be equal to an integral multiple of 2π . The phase condition is $k_o 2nl = 2m\pi$, where the resulting mode number m at a resonant wavelength is $m = (2nl)/\lambda_o$. The mirror separation (the distance between

the two coupling junctions) is l , n is the refractive index of the waveguide, $2nl$ is the optical path length for one round-trip, k_o is equal to $2\pi/\lambda_o$, and λ_o is the free space wavelength of light. In the circular resonator case, $l = \pi D/2$ where D is the diameter of the ring or disk. As the cavity size is decreased, the frequency spacing of adjacent resonant modes increases. The free spectral range, $\Delta\lambda_{\text{fsr}}$, is the spacing of modes separated by a 2π phase difference and given by $\Delta\lambda_{\text{fsr}} = \lambda_{m+1} - \lambda_m = \lambda_{m+1}l/(m+1) - 2n\lambda_m l/m$. If material dispersion is ignored and the resonant wavelengths are very closely spaced such that $\lambda_{m+1} \cong \lambda_m \cong \lambda$, then the $\Delta\lambda_{\text{fsr}}$ is approximated by $\lambda^2/2nl$. The $\Delta\lambda_{\text{fsr}}$ is inversely proportional to the cavity size.

The transmitted intensity I_t is

$$I_t = I_o \frac{(1 - R_1)(1 - R_2)A}{(1 - \sqrt{R_1 R_2}A)^2 + 4\sqrt{R_1 R_2}A \sin^2[\delta/2]} \quad (1)$$

with $A = \exp[-\alpha l]$, where α is the intensity attenuation coefficient. For mirrors of equal reflectivity, the intensity reflection is $R = R_1 = R_2$, where R is equal to 1 minus the waveguide-to-resonator coupling efficiency. In reality, physical fabrication irregularities can cause each of the waveguide-to-resonator gaps to be slightly different, creating asymmetric coupling. In an extreme example, variation of the gap width between 0.1–0.15 μm can cause the TM coupling to vary between roughly 1.5–5% for a 10- μm -diameter disk resonator with 0.5- μm -wide adjacent waveguides. Since “unbalanced” mirrors can degrade the resonator transmission, one approach is to have a resonator that utilizes a wider gap and has less strict fabrication tolerances [12]. In the analysis of these experimental results, we assume that the waveguide-to-resonator coupling is the same on each side and that the mirror reflectivities R_1 and R_2 are equal.

The transmissivity (transmitted flux density distribution) is

$$\frac{I_t}{I_o} = \frac{t_{\text{max}}}{1 + F \sin^2[\delta/2]} \quad (2)$$

where

$$t_{\text{max}} = (1 - R)^2 A / (1 - RA)^2. \quad (3)$$

The coefficient of finesse F equals $4RA/(1 - RA)^2$. As R and A increase (coupling out of the cavity is low and α is low), the linewidth sharpens and the resonant transmission t_{max} is very high. With increasing α and decreasing R , the photon lifetime in the cavity becomes short and the linewidth broadens.

The finesse is

$$\mathcal{F} = \frac{2\pi}{2\delta_{1/2}} = \frac{\pi}{2 \sin^{-1} \left[\frac{1}{\sqrt{1/(2+F)}} \right]} \quad (4)$$

and is typically approximated to $\mathcal{F} = \pi\sqrt{F}/2 = \pi\sqrt{RA}/(1 - RA)$ for large values of the coefficient of finesse F .

The total cavity losses (aside from the evanescent coupling to the adjacent waveguides) can be estimated from the resonator performance and are due to several different

TABLE I
 R AND α CALCULATED FROM THE EXPERIMENTALLY DETERMINED PARAMETERS t_{\max} AND \mathcal{F} . CONSERVATIVE
 ACCURACY ESTIMATES ACCOUNT FOR MEASUREMENT FLUCTUATIONS WITHIN A STANDARD DEVIATION OF 5%

	$t_{\max} = 1 - (r_{\min} \pm 5\%)$	$\mathcal{F} (\pm 5\%)$	R	α (1/cm)
10.5- μm ring (TE)	0.85	4.2	0.50832 + 2.98% / -3.18 %	34.97 -3.24 / +3.54
10.5- μm ring (TM)	0.8	20.1	0.86963 + 3.89% / -4.27 %	10.48 -1.02 / +1.13
10.5- μm disk (TM)	0.5	120	0.98166 + 2.34% / -2.57%	4.88 -0.51 / +0.5%

loss mechanisms. The total intensity attenuation coefficient is expressed here as

$$\alpha_T = \alpha_S + \alpha_L + \alpha_C + \alpha_B \quad (5)$$

where α_S is sidewall scattering loss, α_L leakage loss to the substrate, α_C is the loss due to the scattering or mode mismatch at the resonator-to-waveguide coupling junctions (“mirror losses”), and α_B is curvature-induced bending loss. α_S accounts for radiation losses due to sidewall scattering due to surface imperfections and etching striations. Backscattering in the cavity may also excite the counterpropagating mode and degrade the resonator Q , depending on the distribution and nature of the surface roughness. We have not yet evaluated this backscattering effect experimentally, but it has been solved analytically and shown numerically [13], [14]. The leakage loss coefficient α_L is significantly reduced by increasing the buffer layer between the guiding layer and substrate layer. As seen in Fig. 1(b), we use a 2- μm -thick buffer layer of AlGaAs of which 1.5 μm is etched through. We calculate α_L for the TE and TM modes to be 0.53 and 0.63/cm, respectively, for a 0.35- μm -wide waveguide [15]. For strongly confined disk and ring cavities with 10.5 μm diameters, the bending loss coefficient α_B is negligible [16]. The losses are dominated by α_S and α_C , but the contributions from each cannot be readily separated so the following measurements comprise both.

III. EXPERIMENTAL RESULTS

The waveguide-coupled resonators described here have been successfully patterned and fabricated in epitaxial layers of AlGaAs/GaAs using electron-beam lithography and chemically assisted ion beam etching (CAIBE) [9]. As shown in the scanning electron microscope (SEM) image of Fig. 2(a), the 10.5- μm -diameter ring resonator is composed of 0.35- μm -wide waveguides and a 0.12- μm -wide resonator-to-waveguide gap. The resonators were etched to a depth of 2.2 μm . The narrow ring waveguide was patterned to be 0.4 μm wide and is slightly over-etched due to high proximity effects in the electron-beam lithography and the deep semiconductor material etching. The estimated accuracy of the fabricated parameters and of the measurements of the dimensions under SEM observation is $-0.01/+0.02$ μm . A close-up of the corner of a cleaved waveguide end facet is shown in Fig. 2(b) indicating the high quality of fabrication. The sidewall roughness (vertical striations) is approximately 10 nm, and the surface scattering due to this sidewall roughness is the most significant contribution to the propagation loss in these experimental measurements. The experimental setup uses an end-firing

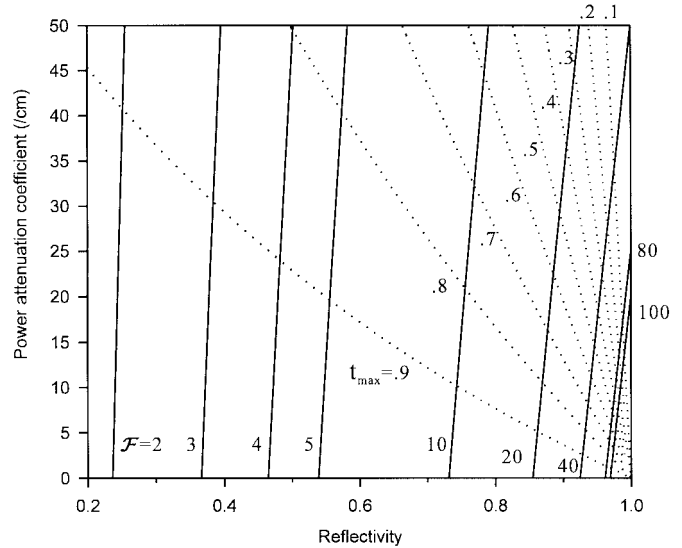
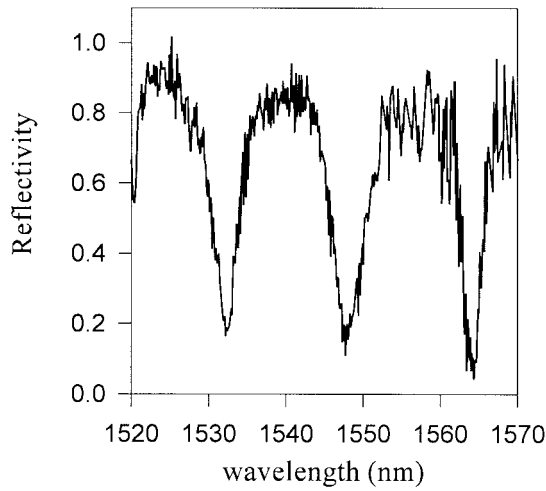


Fig. 3. Power attenuation coefficient α as a function of R for a 10- μm -diameter disk for varying values of t_{\max} and \mathcal{F} .

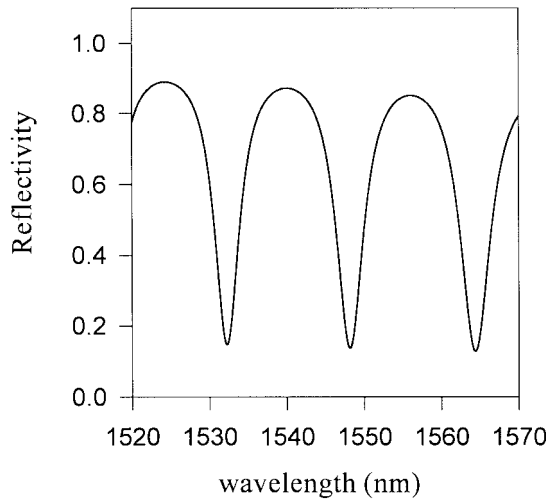
method to couple light into the waveguides by focusing into the input end (port X) and using a second lens to recollimate the light from the output waveguides (port Y or Z). The light source is a narrow linewidth laser diode which is tunable over the 1520–1580-nm range.

Using the experimentally measured values of r_{\min} (minimum resonator reflectivity) and \mathcal{F} , the parameters R and α can be found following (3) and (4). Since the experimental measurements are all reflectivity measurements, the resonator transmissivity, t_{\max} , is determined by $1 - r_{\min}$. The relationship between these parameters is illustrated in Fig. 3 for constant lines of t_{\max} and \mathcal{F} in a 10- μm -diameter cavity. The intersection of the t_{\max} and \mathcal{F} values indicates corresponding values of R and α . The noise in the experimental measurements (due mainly to laser signal fluctuations, and a 1-nm-spaced laser modulation ripple) has a standard deviation of 5%. The following results are provided with accuracy measures that account for combinations of $\pm 5\%$ variations in both r_{\min} and \mathcal{F} that give the worst case errors.

The reflectivity measurements for the 10.5- μm -diameter ring are shown in Fig. 4(a) for TE polarization and Fig. 5(a) for TM polarization. For the 10.5- μm -diameter ring, $R = 0.508$ and $A = 0.94679$ ($\alpha = 35.0/\text{cm}$) for the TE polarization and $R = 0.870$ and $A = 0.98368$ ($\alpha = 0.5/\text{cm}$) for the TM polarization. The results are summarized in Table I and conservative measures of accuracy are provided for $\pm 5\%$ measurement errors in r_{\min} and \mathcal{F} . The cases where the error

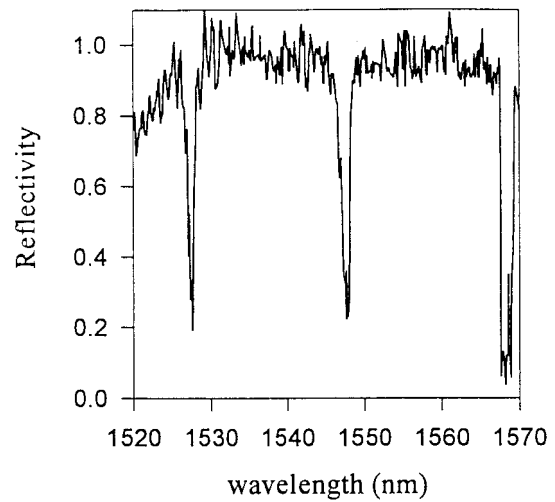


(a)

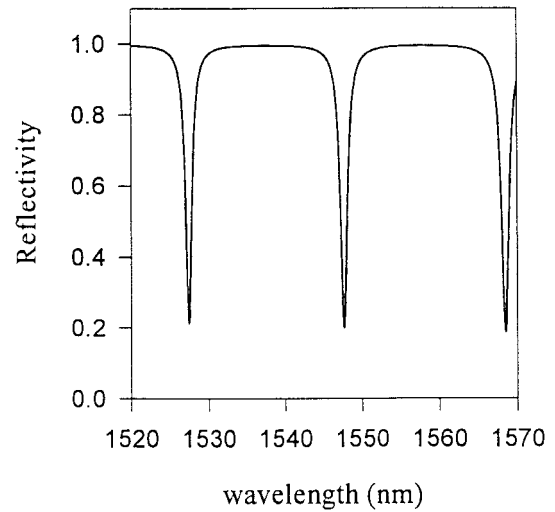


(b)

Fig. 4. (a) Measured reflectivity for TE light from the 10.5- μm -diameter ring and (b) calculated fit.



(a)



(b)

Fig. 5. (a) Measured reflectivity for TM light from the 10.5- μm -diameter ring and (b) calculated fit.

is most significant for loss is when $r_{\min} = r_{\min} + 0.05r_{\min}$ and $\mathcal{F} = \mathcal{F} - 0.05\mathcal{F}$, or when $r_{\min} = r_{\min} - 0.05r_{\min}$ and $\mathcal{F} = \mathcal{F} + 0.05\mathcal{F}$. The percentage error in R is calculated in relation to unity reflectivity and is calculated as $(R - R')/(1 - R)$ where R' is the value with the indicated variations in r_{\min} and \mathcal{F} . Another comparison that is of interest is that of the ring resonator cavity and the disk resonator cavity, and those results are also shown in Table I. The adjacent waveguide is 0.5 μm wide in order to match the fundamental whispering gallery mode width propagating in the disk [9]. As expected, the disk cavity has lower cavity losses than the ring cavity.

The experimentally calculated reflectivities are shown in Fig. 4(b) for TE and Fig. 5(b) for TM. In these calculations, R is calculated as a function of λ following [17]. The amount of waveguide coupling for TE polarization is much higher than TM polarization. The loss for the TE polarization is also much higher than the loss for the TM polarization in these small waveguides. Note that even for such high loss values, the cavity loss is still not high enough to destroy the resonance characteristics due to the very small cavity size. In

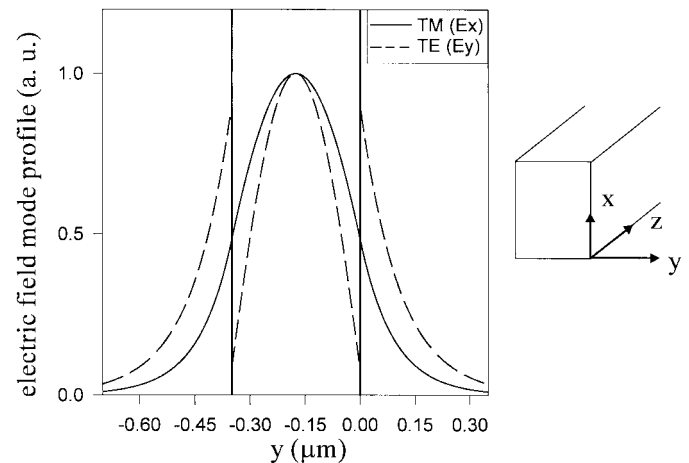


Fig. 6. TE (dashed line) and TM (solid line) intensity mode profiles for the fundamental mode propagating in a 0.35- μm -wide straight waveguide. The cross-sectional view also indicates the waveguide sidewalls at $y = 0$ and $y = 0.35$.

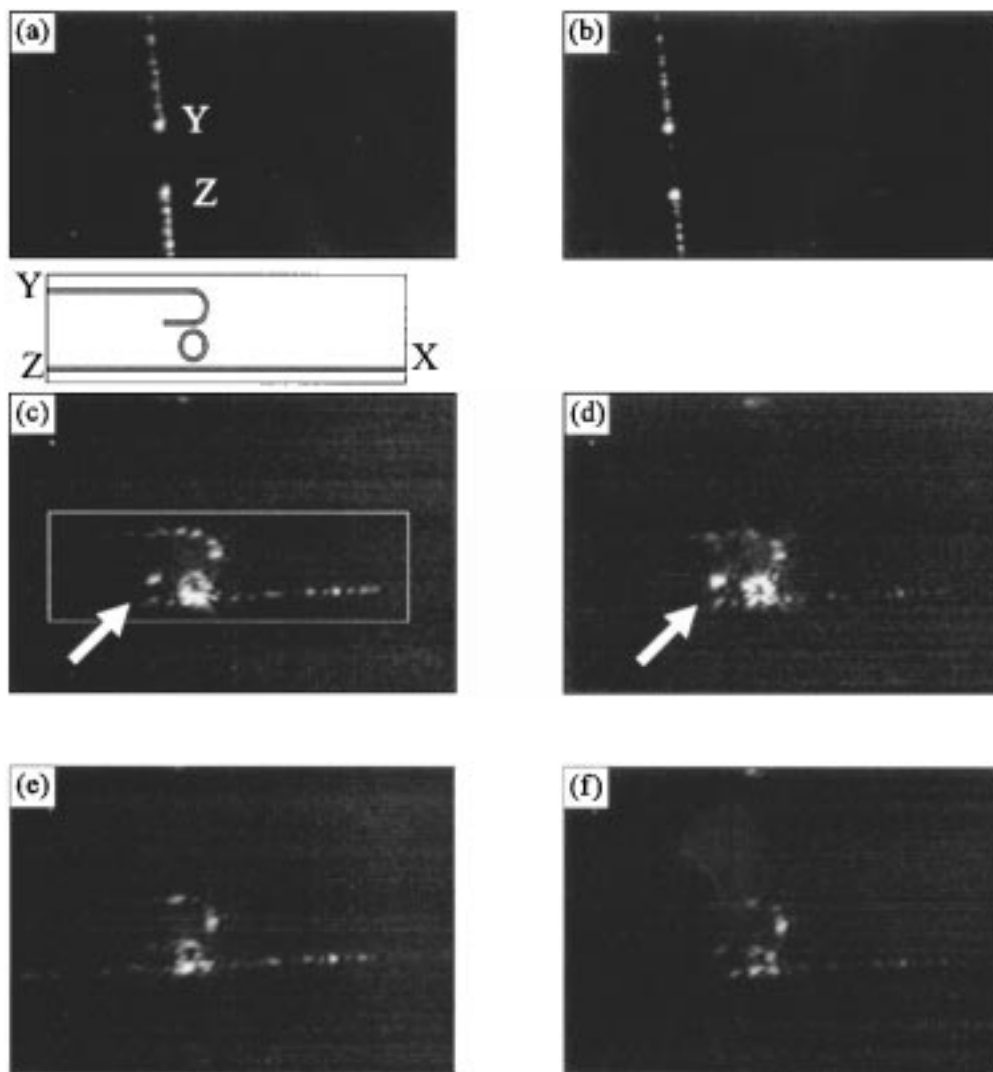


Fig. 7. Infrared camera images showing top views of (a) on-resonance switching of TE-polarized light from the reflection port Y to the transmission port Z and (b) on-resonance switching of TM-polarized light, and top views of the $10.5\text{-}\mu\text{m}$ -diameter ring resonator showing: (c) on-resonance TE, (d) on-resonance TM, (e) off-resonance TE, and (f) off-resonance TM cases. Resonant light switched to WG2 is indicated with an arrow in (c) and (d).

Fig. 6, the intensity mode profiles are calculated as a function of the lateral dimension y using the effective index method. The TE polarization (E_y) profile protrudes farther out of the $0.35\text{-}\mu\text{m}$ -wide-waveguide sidewall than the TM polarization (E_x). The intensity distribution leads to higher waveguide-to-resonator evanescent coupling as well as higher sidewall scattering losses for the TE polarization.

In the infrared camera images of Figs. 7 and 8, top views of the ring and disk resonators are shown as the polarization of the light is changed from TM (electric field out of the page) to TE (electric field parallel to the page) for on- and off-resonance cases. For the ring case, the adjacent waveguides and the ring-cavity waveguides are all $0.35\ \mu\text{m}$ wide. In these figures, the increased sidewall scattering of the TE-polarized light is visible along the adjacent waveguide. In the on-resonance cases, the intensity of the light building in the disk or ring cavity is evident in the amount of scattering from the cavity. The ring resonator waveguide outputs (ports Y and Z) are shown in Fig. 7(a) and (b) for on-resonance light of the TE and TM cases, respectively. In Fig. 7(c) and (d), the

on-resonance light (indicated with an arrow) is seen exiting one end of the transmission waveguide WG2 for the TE and TM cases. In Fig. 7(e) and (f), infrared images are shown for the off-resonance cases of TE and TM polarizations. The small dot of light shown at the curved portion of WG2 is observable in all the images and is not scattered on-resonant light from WG2. It is light that is traveling in the un-etched portion of the sample that scatters when it hits the etched waveguide feature. (The resonator and waveguide features are created and isolated by etching a $1\text{-}\mu\text{m}$ -wide trench around the features, leaving other areas un-etched. The un-etched areas can act as a slab waveguide, guiding some of the light that is not coupled into the resonator input waveguide.)

The infrared camera images in Fig. 8 show top views of the $10.5\text{-}\mu\text{m}$ -diameter disk for the a) on-resonance TM-polarized light, b) off-resonance TM-polarized light, and c) off-resonance TE-polarized light. There were no strong resonances observed in the disk resonator for the TE case due to the very high TE propagation loss in the resonator as compared to the small amount of waveguide-to-resonator coupling. For the

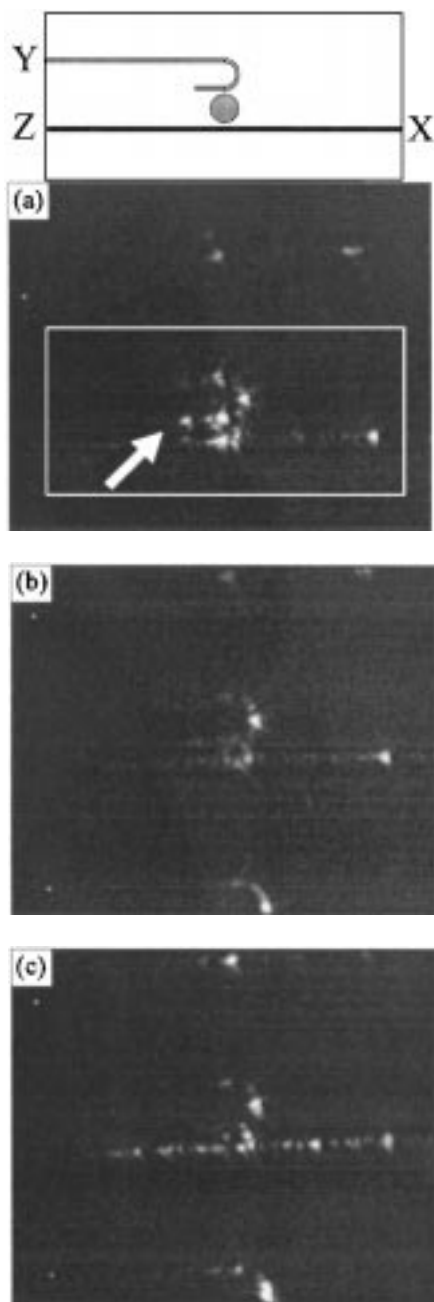


Fig. 8. Infrared camera images showing top views of the 10.5- μm -diameter disk resonator showing (a) on-resonance TM, (b) off-resonance TM, and (c) off-resonance TE cases. Resonant light switched to WG2 is indicated with an arrow in (a).

TE polarization, the increased scattered light from waveguide surface imperfections is evident in the infrared images of Fig. 8.

IV. CONCLUSION

With the advancement of nanoscale photonic devices and the potential for planar integration of photonic circuits, there is an increasing need for high quality, single-mode, strongly guiding waveguides and the devices based on them. We report loss measurements in 10.5- μm -diameter ring cavities composed of strongly confined, submicron waveguide struc-

tures. The ring resonator is created in AlGaAs/GaAs using nanofabrication techniques, and the GaAs core has an area of 0.1575 μm^2 . Power attenuation losses are reported for TE and TM electric field polarizations in ring resonator structures with good measures of accuracy. Relatively low power attenuation coefficients of 4.88/cm are reported for disk structures, indicating an advantage for disk resonators over more conventional ring resonators. As the design and fabrication of this novel microcavity resonator are further optimized, the resonator performance is expected to improve to the level of practical commercial applications.

REFERENCES

- [1] J. Haavisto and G. A. Pajer, "Resonance effects in low-loss ring waveguides," *Opt. Lett.*, vol. 5, pp. 510–512, Dec. 1980.
- [2] R. Adar, Y. Shani, C. H. Henry, R. C. Kistler, G. E. Blonder, and N. A. Olsson, "Measurement of very low loss silica on silicon waveguides with a ring resonator," *Appl. Phys. Lett.*, vol. 58, pp. 444–445, Feb. 1991.
- [3] T. Kominato, Y. Ohmori, N. Takato, H. Okazaki, and M. Yasu, "Ring resonators composed of GeO₂-doped silica waveguides," *J. Lightwave Technol.*, vol. 10, pp. 1781–1787, Dec. 1992.
- [4] W. J. Wang, S. Honkanen, S. I. Najafi, and A. Tervonen, "New integrated optical ring resonator in glass," *Electron. Lett.*, vol. 28, pp. 1967–1968, Oct. 1992.
- [5] R. Adar, M. R. Serbin, and V. Mizrahi, "Less than 1 dB per meter propagation loss of silica waveguides measured using a ring resonator," *J. Lightwave Technol.*, vol. 12, pp. 1369–1372, Aug. 1994.
- [6] W. Weiershausen and R. Zengerie, "Photonic highway switches based on ring resonators used as frequency-selective components," vol. 35, pp. 5967–5978, Oct. 1996.
- [7] Y. Hida, S. Imamura, and T. Izawa, "Ring resonator composed of low loss polymer waveguides at 1.3 μm ," *Electron. Lett.*, vol. 28, pp. 1314–1316, July 1992.
- [8] D. Rafizadeh, J. P. Zhang, S. C. Hagness, A. Taflove, R. C. Tiberio, K. A. Stair, and S. T. Ho, "Nanofabricated waveguide-coupled 1.5- μm microcavity ring and disk resonators with high Q and 21.6-nm free spectral range," in *Proc. Conf. Lasers Electro-Optics*, Baltimore, MD, postdeadline paper CPD23, May 1997.
- [9] ———, "Waveguide-coupled AlGaAs/GaAs microcavity ring and disk resonators with high finesse and 21.6-nm free spectral range," *Opt. Lett.*, vol. 22, pp. 1244–1246, Aug. 1997.
- [10] J. S. Foresi, B. Little, G. Steinmeyer, E. Thoen, S. Chu, H. Haus, E. Ippen, L. Kimmerling, and W. Greene, "Si/SiO₂ micro-ring resonator optical add/drop filters," in *Proc. Conf. Lasers Electro-Optics*, Baltimore, MD, postdeadline paper CPD22, May 1997.
- [11] F. C. Blom, D. R. van Dijk, H. J. W. M. Hoekstra, A. Driessen, and Th. J. A. Popma, "Experimental study of integrated-optics microcavity resonators: Toward an all-optical switching device," *Appl. Phys. Lett.*, vol. 71, pp. 747–749, Aug. 1997.
- [12] S. C. Hagness, D. Rafizadeh, S. T. Ho, and A. Taflove, "FDTD analysis and comparison of circular and elongated ring designs for waveguide-coupled microcavity ring resonators," in *Proc. Integrated Photon. Res. Conf.*, Victoria, B.C., Canada, Mar. 1998.
- [13] ———, "FDTD microcavity simulations: Design and experimental realization of waveguide-coupled single-mode ring and whispering-gallery-mode disk resonators," *J. Lightwave Technol.*, vol. 15, pp. 2154–2165, Nov. 1997.
- [14] B. E. Little and J.-P. Laine, "Surface-roughness-induced contradirectional coupling in ring and disk resonators," *Opt. Lett.*, vol. 22, pp. 4–6, Jan. 1997.
- [15] W. Stutius and W. Streifer, "Silicon nitride films on silicon for optical waveguides," *Appl. Opt.*, vol. 31, pp. 3218–3222, Dec. 1977.
- [16] E. A. J. Marcatili, "Bends in optical dielectric guides," *Bell. Syst. Tech. J.*, vol. 48, pp. 2103–2132, Sept. 1969.
- [17] ———, "Dielectric rectangular waveguide and directional coupler for integrated optics," *Bell. Syst. Tech. J.*, vol. 48, pp. 2071–2012, Sept. 1969.

D. Rafizadeh, photograph and biography not available at the time of publication.

J. P. Zhang, photograph and biography not available at the time of publication.

S. T. Ho, photograph and biography not available at the time of publication.

R. C. Tiberio, photograph and biography not available at the time of publication.